Journal of Hydrology 572 (2019) 388–402

Contents lists available at ScienceDirect

Journal of Hydrology

journal homepage: www.elsevier.com/locate/jhydrol

Research papers

Impact-based flash-flood forecasting system: Sensitivity to high resolution numerical weather prediction systems and soil moisture

F. Silvestro[a,*], L. Rossi[a], L. Campo[a], A. Parodi[a], E. Fiori[a], R. Rudari[a], L. Ferraris[a,b]

[a] CIMA Research Foundation, Savona, Italy
[b] University of Genova, Genova, Italy

ARTICLE INFO

This manuscript was handled by Marco Borga, Editor-in-Chief

Keywords:
Flood Forecast
Probabilistic
Damage
Impacts
Hydrometeorology

ABSTRACT

In recent years, continuous improvements have been made in weather forecasting and flood prediction with great benefit from Early Warning Systems (EWSs). Despite the continuous quest for innovation from the scientific and user communities, EWSs remain based mostly on hazard forecast, and the information on possible consequences and potential impacts is generally missing.

In this work, a methodology for quantitative real-time impact assessment for flash floods is presented. The methodology uses a multi-model ensemble approach and considers soil moisture uncertainty. Moreover, the flood forecasting chain, which normally provides only the discharge probability of exceeding a given threshold, is extended to include a fully 2D hydraulic model and a damage estimation model to quantitatively assess impacts in terms of economic losses and the people involved.

The procedure was tested on recent flood events occurring in Genoa in northwestern Italy. This paper discusses the potential challenges and opportunities offered by this approach in the decision-making workflow in an operational context.

1. Introduction

Despite continuous improvements in weather forecasting and flood prediction, floods still cause multiple casualties and significant damage to properties and infrastructures every year with adverse economic consequences for communities that can persist for many years. This trend may worsen in the future, if we consider the effects of climate change and urbanization. According to a recent study of the European Environment Agency (EEA, 2016), annual flood losses can be expected to increase fivefold by 2050 and up to 17-fold by 2080.

Rarely, hydro-meteorological forecasts are connected to quantitative potential impact estimates (economic losses and people involved), since hydro-meteorological forecasts are generally devoted to prediction of possible flood magnitudes (Silvestro et al., 2011; Gourley et al., 2014, 2017; Naulin et al., 2013; Versini et al., 2014). As a consequence, decisions from the authorities responsible for civil protection/emergency management are based on the experience accumulated by the forecasters using their technological systems, while actions to safeguard population and assets are often determined by their subjective perception of the local risk conditions. While there is a realization of what the weather might be, there is frequently a lack of understanding of what the weather might do (WMO, 2015).

To improve Early Warning Systems (EWSs), a paradigm to shift from hazard to impact forecasts is needed. Recent studies proposed methodologies for rapid impact assessment and estimation of damage severity (Schroeder et al., 2016; Cole et al., 2016; Sai et al., 2018) or direct estimation of the number of impacted buildings (Le Bihan et al., 2016; Le Bihan et al., 2017). The economic dimension, when addressed, is often computed at a coarse resolution (Dottori et al., 2017), incompatible with flash-flood impact assessment needs.

The present approach goes one step further by computing direct economic damage and impact on the population at a building scale, which will ultimately result in better contingency planning (reasonable worst-case and most likely outcomes). The decision-making process will be facilitated and put under a cost-benefit perspective (e.g., economic losses of the predicted event may be quantitatively compared to the cost of mitigation measures). This approach would also improve the objective evaluation of responsibilities of forecasters and decision makers in the EWS context. Additionally, impact forecasts can contribute to a common situational awareness and a better acceptance of mitigation countermeasures by the general public.

The enhancement process of an Early Warning System relies, on one hand, on improving the quality of hazard forecasts by quantifying major sources of uncertainty and, on the other hand, on extending the

* Corresponding author.
E-mail address: francesco.silvestro@cimafoundation.org (F. Silvestro).

https://doi.org/10.1016/j.jhydrol.2019.02.055
Received 25 July 2018; Received in revised form 15 January 2019; Accepted 14 February 2019
Available online 02 March 2019

modelling chain to quantitatively assess potential losses.

These two principles have been applied to improve the Flash Flood Early Warning System for the city of Genoa, which recently suffered the consequences of two devastating flash floods in 2011 and 2014 (Fiori et al., 2014, 2017, Silvestro et al., 2012).

Many modelling experiments based on forecasting chains (Davolio et al., 2015, Hally et al., 2015; Davolio et al., 2017) have been conducted in recent years to evaluate the amount of hydrometeorological uncertainty in the prediction of the flash floods that hit the Ligurian region on the northwest side of Italy (hereafter the Liguria region). One of the most recent studies (Parodi et al., 2017) was supported by the use of a prototype Distributed Computing Infrastructure (DCI) developed under the EU-funded projects DRIHM (Distributed Research Infrastructure for Hydro-Meteorology, www.drihm.eu) and DRIHM2US (Distributed Research Infrastructure for Hydro-Meteorology to US, www.drihm2 μs.eu) for studying high impact weather events (HIWEs) with a special focus on floods and flash-flood events.

Based on the experience mentioned above, this work addresses three main topics. The first topic is the evaluation of possible added value of high-resolution numerical weather prediction systems (NWPSs) as input for streamflow forecasts on a study area characterized by a small basin struck by flash-flood events (Davolio et al., 2015; Fiori et al., 2017). The second is understanding how the uncertainties in the initial soil moisture conditions of the hydrological model can affect the forecast performance (Silvestro and Rebora, 2014). The third is extending the typical flood forecasting chain (rainfall-discharge-water levels) to quantitatively include exposure and vulnerability factors and understanding how the first two topics interact and affect the forecast in terms of impacts. The analysis of flood events based on stream flow only predicts the probability of overtopping but does not provide quantitative information on the affected population and properties (Molinari and Handmer, 2011; Sättele, 2016). The formulation of impact scenarios is necessary to better understand the consequences of a forecast event, and then to apply mitigation measures in real time as foreseen in emergency plans.

Hazard predictions expressed as probabilistic maps of flood water depth and velocity are thus translated into impact predictions, such as the probability of exceeding a given economic loss or the probability that a certain number of people can be affected by the flood.

2. Materials and methods

2.1. Study area and case studies

Bisagno is a basin located in northwestern Italy in the Liguria Region. The drainage area is small (approximately 98 km^2), and the elevations of the catchment range between 0 and 1100 m above sea level, so the environment changes from mountainous to coastal with high slopes (Fig. 1) in few kilometres; the mean catchment elevation is approximately 370 m. Bisagno is mainly covered by forests and brushes, but with a high level of urbanization along the last 10 km of the riverbed, which is characterized by a high concentration of inhabited areas, industries and other infrastructure highly prone to the risk of flooding because the city developed along the Bisagno River bed from the outlet to the inland during the last century. Furthermore, along the last 1.5 km, the river flows underneath a heavily urbanized area, and the maximum discharge under the conditions of free surface flow is approximately 700 m^3/s (which corresponds to a return period $T < 30$ y). Streamflow values larger than the latter threshold cause a sudden reduction of the maximum discharge carried under the cover and the flow overbanking.

Liguria is monitored through a meteo-hydrological network named OMIRL–"Osservatorio Meteo-Idrologico della Regione Liguria" as described in Silvestro et al. (2015a). This network is the official network of the Liguria Region, which contributes to the Italian micro-meteorological network operationally used by the Italian Civil Protection Department (Molini et al., 2009). The stations furnish measurements with a time step of 5–10 min. There are approximately 200 rain gauges over the region with an average density of 1 rain gauge/40 km^2; the network also has stations with other sensors (temperature, radiation, wind, air humidity, etc.), but in these cases, the densities are lower than the rain gauge density. The instruments are professional tipping bucket gauges with 0.2 mm accuracy, maximum error with an intensity of 300 mm/h of approximately 2%, and they satisfy all the WMO recommendations and are regularly maintained by the regional technicians.

The Bisagno basin is particularly well-instrumented: the rain-gauge network density is approximately 1 rain gauge/10 km^2.

A water level station named Passerella Firpo is located near the beginning of the cover and has an upstream area of approximately 93 km^2; level data can be used together with an available stage-discharge curve to estimate observed streamflow.

Three extreme rainfall events are considered for the presented analysis based on the following reasons:

1. Two events caused inundation with severe damages, while the third event caused a streamflow that was very close to the flooding level (Table 1).
2. These events exhibited the typical thermodynamic and kinematic features related to the occurrence of V-shaped back-building Mesoscale Convective Systems in the Liguria sea area (Rebora et al., 2013, Silvestro et al., 2015, Fiori et al., 2014, 2017; Lagasio et al., 2017);
3. The results of the operational forecasting chain applied to these case studies are available to verify the quality of the new approach.

2.2. Impact-flood forecast modelling chain

The impact forecast modelling chain hereinafter proposed to extend the typical flood forecasting chain (Hally et al., 2015) that furnishes results in terms of streamflow, by adding one module for hazard spatialization (flooded areas expressed in terms of water depth and velocity) and one for damage computation.

As shown in Fig. 2, the final modelling chain is formed by several modelling blocks: meteorological multi-models at global and limited area scale, a stochastic downscaling model, a fully distributed hydrological model, a fully 2D hydraulic model and a damage model.

2.2.1. NWPS: benchmark and high-resolution models

The numerical weather prediction system (NWPS) used in the study consists of three different non-hydrostatic models: HARMONIE-AROME model, MOLOCH and WRF-AWR model.

The HIRLAM–ALADIN Research on Mesoscale Operational NWP in Euromed (HARMONIE) model is a convection-permitting model developed by Météo-France and ALADIN. This model is generally nested in the European Centre for Medium-Range Weather Forecasts (ECMWF) global model, and it uses the same non-hydrostatic (NH) dynamic core as AROME-France. Bengtsson et al. (2017) describe the model setup and its similarities- differences with respect to the AROME-France model: with respect to the shortwave (SW) radiation parameterization, the Morcrette radiation scheme with an improved cloud liquid optical property scheme (Nielsen et al., 2014) is implemented. The microphysics scheme used is a one-moment bulk scheme, which uses a three-class ice parameterization (ICE3) while a new turbulence scheme, HARMONIE with RACMO Turbulence (HARATU), is available. No parameterization is employed for deep convection, while a so-called eddy diffusivity mass-flux (EDMF) parameterization is used for shallow convection. The cycle 40 h1.1 of the HARMONIE-AROME is used for this study with 2.5 km grid spacing and 65 vertical model levels extending up to 10 hPa.

MOLOCH is a fully compressible, convection-permitting model (Morrison and Pinto, 2006; Davolio et al., 2015) developed at the

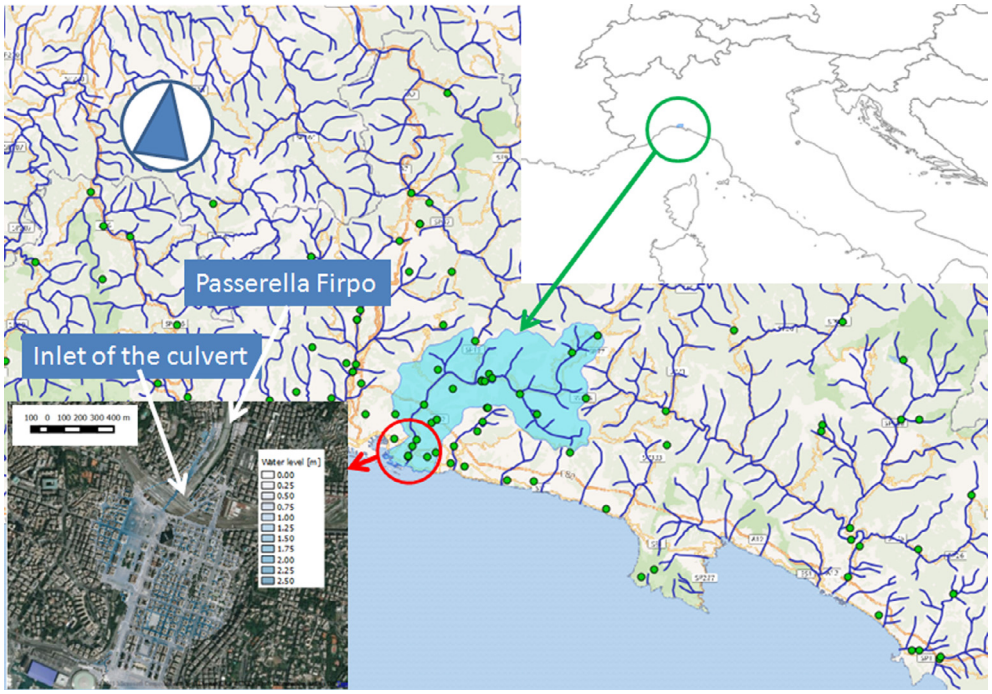

Fig. 1. Study area. In light blue, the watershed of the Bisagno Basin. Green points are the rain gauges, red lines represent the regional boundaries while grey lines are the main stream lines. Bottom left panel shows the zoom on the city of Genoa in the area where inundation frequently occurs and the Passerella Firpo level gauge. An example of the inundation map is also reported (event on 09/10/2014). (For interpretation of the references to colour in this figure legend, the reader is referred to the web version of this article.)

Table 1
Main characteristics of the three events considered. Max rainfall 24 h and Max rainfall 1 h are the maximum accumulated rainfall for 24 and 1 h, respectively, measured by a gauge located in the catchment. Peak flow is the maximum observed streamflow measured through the level gauge of Passerella Firpo.

Event	Max rainfall 24 h [mm]	Max rainfall 1 h [mm]	Duration [hours]	Peak flow [$m^3 s^{-1}$]
04/11/2011	550	142	13	830
09/10/2014	400	130	8	1150
14/09/2015	258	73	6	610

Institute of Atmospheric Sciences and Climate of the Italian National Research Council (CNR-ISAC) and is operationally combined with the BOLAM model from which it receives hourly lateral boundary information (www.isac.cnr.it/dinamica/projects/forecasts). The model settings for radiation, turbulence and microphysics schemes used here are those of Davolio et al. (2015). The MOLOCH operational configuration (until the year 2017) has a grid spacing of 2.3 km and 50 vertical levels. It is operational at the Functional Centre for Meteo-Hydrological of the Liguria Region, which is the institution in charge of making flood forecasting on the study area. For this reason, it is considered as the main Benchmark in this study. This choice was done to make a comparison between what the forecaster had as information

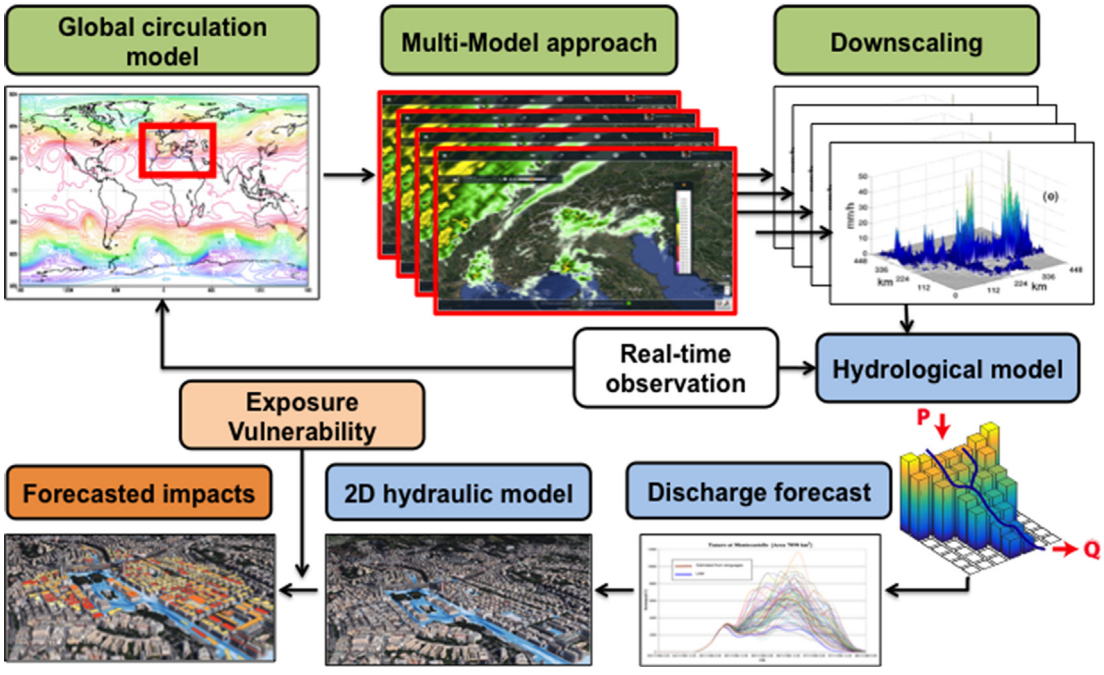

Fig. 2. Conceptual scheme of the damage forecast probabilistic modelling chain.

before the event and what the forecaster would have had if the system analysed in this work had been available.

The Advanced Research Weather Research and Forecasting (WRF, version 3.7) model is a fully compressible regional atmospheric model, with terrain following the hydrostatic pressure vertical coordinate. The WRF setup implemented here starts from the modelling results in Lagasio et al. (2017): two nested domains with, respectively, 5 km and 1 km grid spacings are used with the total numbers of vertical levels of 50 over the 20-km atmosphere depth. Explicit treatment of convection is adopted while four different types of microphysics are used for each case: the WRF single-moment six-class scheme (WSM6) (Hong and Lim, 2006), Thompson (Thompson et al., 2008), WRF double moment 6-class scheme (Lim et al., 2010), hereafter WDM16, and Morrison's double-moment six-class scheme (Morrison and Pinto, 2005, 2006). All the analyses presented hereafter refer to the innermost domain at 1 km grid spacing.

The global operational ECMWF-IFS NWP model (Simmons et al., 1989) with 0.125° of grid spacing valid at 0000 UTC of the same day of each event is used to initialize the three meteorological models.

2.2.2. From meteorological to hydrological forecast: rainfall downscaling and hydrological models

The hydrological modelling suite adopted in this study is described in detail in Silvestro et al. (2015a) and Silvestro et al. (2016), and it consists of a rainfall downscaling model, RainFARM (Rebora et al., 2006a, 2006b), and a hydrological model, Continuum (Silvestro et al., 2013). RainFARM is a rainfall downscaling algorithm that produces an ensemble of rainfall scenarios that maintain some characteristics of the rainfall prediction derived by an NWPS (Laiolo et al., 2014) and can mimic the small-scale variability of precipitation needed to correctly force the hydrological model. The volume of precipitation predicted by the NWPS is preserved by RainFARM, together with the spatial and temporal structure at space and time scales that are considered reliable (S_r, t_r) following the approach described in Siccardi et al. (2005), but each precipitation scenario reproduces a small spatial-temporal variability that is present in a real rainfall field and that can be observed, for example, with meteorological radar as shown in Rebora et al. (2006b).

The spatial-temporal Fourier spectrum of the rainfall field follows the functional form:

$$\hat{g}\,(k_X,\, k_y,\, \omega)^2 \propto (k_X^2 + k_y^2)^{-\alpha/2}\omega^{-\beta} \tag{1}$$

k_x and k_y are the spatial wavenumbers of the × and y directions, ω the temporal wavenumber (frequency), and α and β represent two parameters of the model that are estimated from the power spectrum of rainfall forecast through the NWPS.

In this application, the reliable spatial and time scales (S_r, t_r) are assumed 10*Δx km (where Δx is the horizontal resolution of the NWPS considered) and 6 h based on the experience of Rebora et al. (2006b), Brussolo et al. (2008) and Davolio et al. (2015), and considering that a meteorological model, due to numerical diffusion, is generally not reliable at scales smaller than six to four times its resolution (Patterson and Orszag, 1971). Therefore, RainFARM is constrained to keep the spatial and temporal patterns at these latter scales. The final downscaled rainfall fields have a spatial resolution of 1 km and a time resolution of 60 min.

The rainfall scenarios built with RainFARM are used to feed *Continuum,* which is a distributed hydrological model based on a geomorphologic approach (Giannoni et al., 2005). Continuum combines semi-empirical and physically based modules, and it can work in a continuous way; all the main physical processes that describe the hydrological cycle are modelled (i.e., surface and sub-surface flow, deep flow, infiltration, evapotranspiration, vegetation interception, snow melting and accumulation). A detailed description of the model can be found in Silvestro et al. (2013, 2015b).

A Digital Elevation Model (DEM) is used to represent the catchment morphology, and the flow directions are estimated calculating the directions of maximum slope. Each cell of the model drainage network is classified as hillslope or channel using a morphologic filter defined by the expression

$$A \cdot S^k = C \tag{2}$$

where

- A is the contributing area upstream of each cell [L^2],
- S is the local slope [–],
- k and C are quantities that describe the geomorphology of the basin (Giannoni et al., 2000), and they are generally constant.

Infiltration process and subsurface flow (Gabellani et al., 2008) are modelled using a scheme based on a layer of reservoirs that represents the root-zone (Silvestro et al., 2013) and include a modification of the Horton algorithm (Bauer, 1974; Diskin and Nazimov, 1994). The energy balance is computed using the "force restore equation" approximation (Dickinson, 1988) that allows us to estimate as explicit output variables the soil surface temperature and the evapotranspiration.

The surface flow on hillslope cells is modelled using a linear reservoir scheme while flow on channel cells exploits the kinematic wave approach (Wooding, 1965; Todini and Ciarapica, 2001).

Continuum requires calibration for six parameters, generally carried out at the basin scale: two for the surface flow (u_h and u_c), two for the sub-surface flow (c_t and c_f) and two for deep flow and water-table (V_{Wmax} and R_f) processes. Table 2 reports a brief description of the parameters.

For the current application, the same implementation of Davolio et al. (2017) is used. The model was implemented with a spatial resolution of 0.005 deg (approximately 480 m) based on the Shuttle Radar Topographic Mission (SRTM) DEM and the use of a CORINE Land Cover (http://www.sinanet.isprambiente.it/it/progetti/corine-land-cover-1). The temporal resolution used in all the experiments is 60 min. In Davolio et al. (2017), a parameter calibration that focussed on the flood reproduction was also employed. In this application, the hydrological simulations always start in the coincidence of the date of initialization of the NWPS as shown in Table 3.

2.2.3. Accounting for soil moisture initial condition uncertainty

The considered hydrological model is distributed and continuous. Therefore, it is possible to produce an initial moisture condition at the beginning of each event that is derived by the physical processes simulated inside the model (infiltration, gravity percolation, evapotranspiration); to accomplish this, we carried out a run of the model starting from 01/01/2011 until 12/12/2015 fed by observations. The approach mentioned above should allow the reproduction of a realistic soil moisture pattern, or at least a soil moisture estimation compatible with the model structure when the model is well calibrated. In any case, it is well known (Zappa et al., 2011; Silvestro and Rebora, 2014; Laiolo et al., 2016) that sometimes the modelled soil moisture can be highly different from the real soil moisture, depending on a number of factors,

Table 2
Summary of the model parameters that need calibration with their brief description.

Parameter	Description
u_h [s^{-1}]	Flow motion coefficient in hillslopes
u_c [$m^{0.5}s^{-1}$]	Friction coefficient in channels
c_f [–]	Defines the infiltration capacity at saturation
c_t [–]	Defines the mean field capacity
R_f [–]	Related to anisotropy between the vertical and horizontal saturated conductivity and to soil porosity
V_{Wmax} [mm]	Maximum water capacity of the aquifer in the whole investigated area

Table 3
Time of peak flow and time of initialization of NWPS and hydrological model for each one of the 3 events.

Time to Peak Flow (UTC)	Initialization of NWPS and Hydrological Model
04/11/2011 13:00	03/11/2011 00:00
09/10/2014 22:00	09/10/2014 00:00
14/09/2015: 01:00	13/09/2015: 00:00

e.g., i) ability of the model to reproduce the physical phenomena in a particular simulation time window; ii) reliability of the parameterization in that particular simulation period; and iii) reliability in the forcing data used to drive the model (some variables such as solar radiation or wind are often poorly sampled by the ground gauge network).

A wrong soil moisture initial condition can thus cause over- or under-estimation of the streamflow prediction; the over- or under-estimation can be evaluated in a post event analysis, but it is a-priori unknown.

In the presented analysis, the uncertainty related to the hydrological model parameters was neglected essentially for two reasons. On one side, we used a hydrological model calibrated to reproduce high flows with good performance in reproducing these latter (Davolio et al.; 2017). On the other side, various studies (Mascaro et al., 2010; Zappa et al., 2011) indicated that parameter uncertainty is generally of lower magnitude with respect to uncertainties related to the rainfall forecast and to the initial wetting conditions, especially for small catchments with a flash-flood regime.

To introduce the impact of soil moisture uncertainty, we generated a set of K soil moisture initial conditions starting from the one modelled with the observed meteorological variables. Being Continuum, a continuous distributed model, produces the modelled state variables for each time step of the run made with observations as input. In the case of soil moisture, it is a two-dimensional field with the same spatial resolution as the model implementation (in this case, 0.005 deg).

The mean soil moisture at basin scale (with a value between 0 and 1) can easily be estimated as the mean of the values in the single pixels (here after MSo).

Once the MSo is estimated, to account for possible modelling errors, the set of K soil moisture initial condition is generated with the following steps:

1. The kth mean soil moisture initial condition MSk is extracted from a uniform distribution in the range [MSo-dMS, MSo + dMS], where dMS is set to 0.4; this is an arbitrary value based on previous analysis and on the comparison with satellite estimation (Laiolo et al., 2016; Cenci et al., 2016) and means that we assumed that the maximum variability of the model soil moisture around MSo is 40% of the soil moisture maximum range [0; 1].
2. The ratio:

$$dRatioSM = \frac{MSk}{MSo} \quad (3)$$

is estimated and used to re-scale the soil moisture map, allowing us to change the mean soil moisture at the basin scale, preserving the soil moisture pattern. In this way, it is assumed that the spatial pattern is generally well reproduced by the model

The K soil moisture initial conditions can be combined with the M forecast rainfall fields generated with RainFARM and used to trigger the Continuum model to produce MxK streamflow scenarios.

The perturbations applied to the original soil moisture field affect the internal coherence of the state variables, specifically those related to the energy balance, but this has no important consequences on the results on the time horizon of the forecast (2–3 days). The energy balance negligibly affects the mass balance during such small periods.

2.2.4. Hydraulic modelling, damages and potential affected population scenarios

The 2D hydraulic model used in this work is TELEMAC 2D, which belongs to the TELEMAC-MASCARET (http://www.opentelemac.org/) suite of models to be used for hydraulic modelling applications.

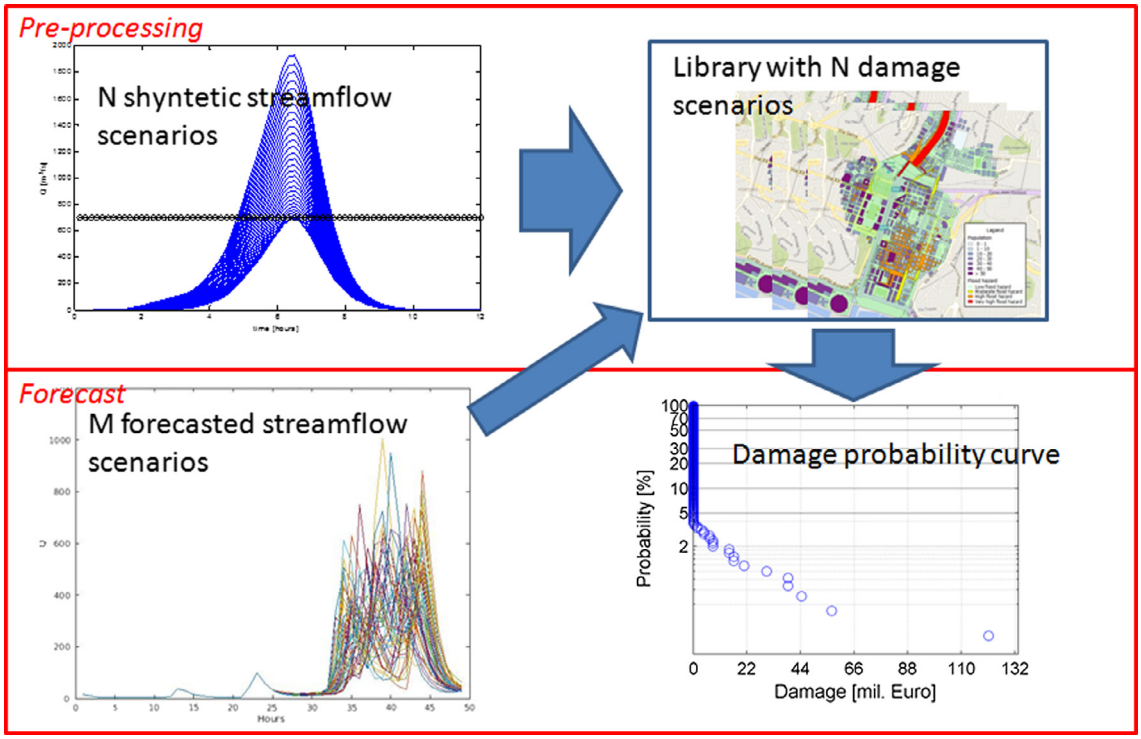

Fig. 3. Scheme that reproduces the system to link pre-processing data with the flow forecast of a particular event. N synthetic streamflow scenarios are used to produce a library of damage scenarios. During the forecast, each of the M streamflow scenarios is compared with the N synthetic scenarios to estimate the related damage.

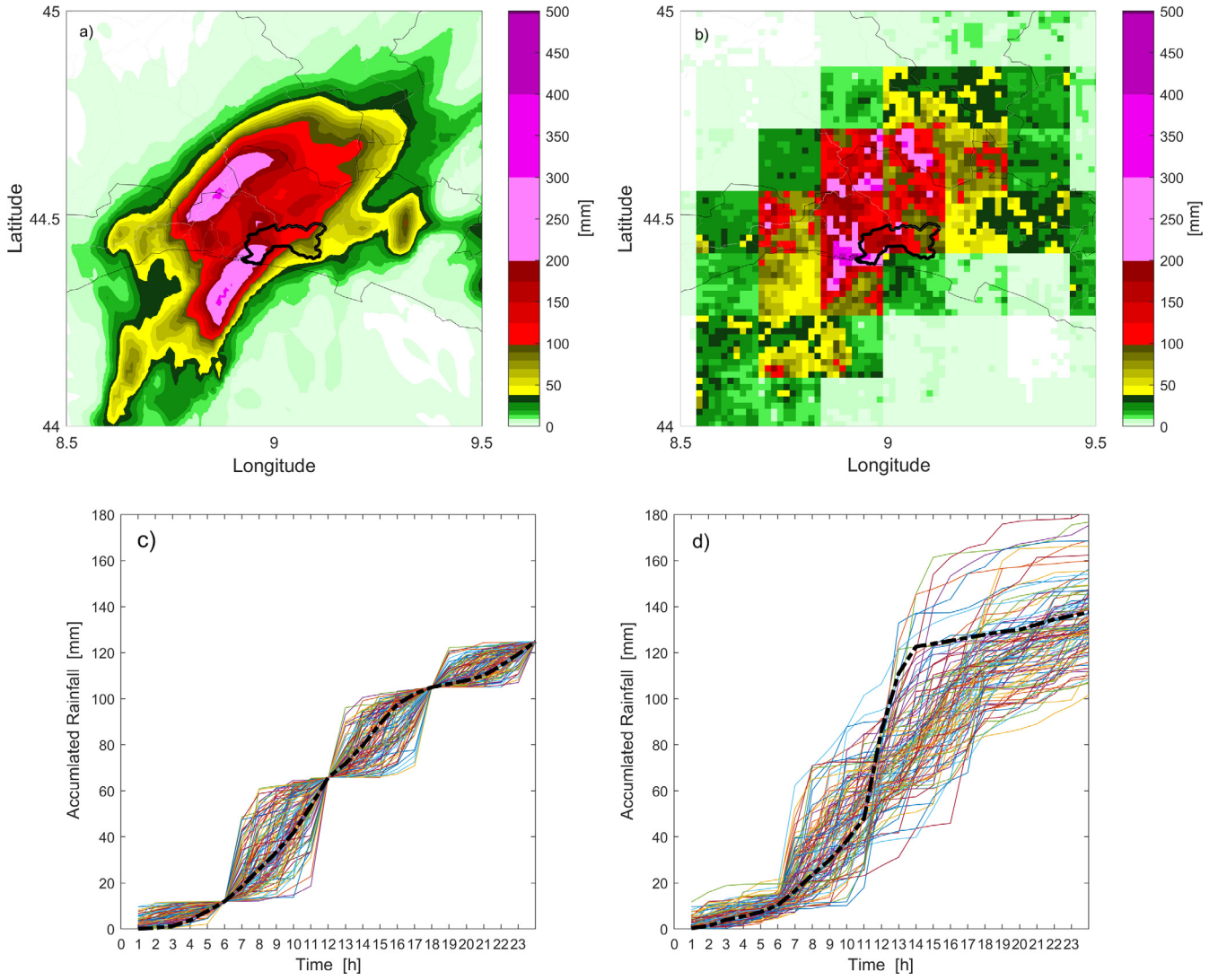

Fig. 4. Example of rainfall downscaling event on 09/10/2014, NWPS: WRF – WSM6. Al panels refers to accumulated rainfall on 24 h between 09/10/2014 00:00 UTC and 10/10/2014 00:00 UTC. Panel a) shows the original rainfall field forecast with WRF-WSM6 and b) shows an example of a downscaled scenario. Panel c) average precipitation accumulated on a box with dimension 2*S_r. Panel d) average precipitation accumulated on the Bisagno Catchment.

TELEMAC 2D is based on the solution of the Saint-Venant equations on a grid of triangular elements, using as numerical schemes the finite-element or finite-volume methods. The ability to model both permanent and transient conditions allows a number of operational and research applications.

In this application, the same setup shown in Silvestro et al. (2016) was used. The hydraulic model was calibrated to model historical flooding accurately, with a special focus on the one that occurred on 09/10/2014. For this event, the large availability of field measurements allowed a good estimation of the magnitude of the flood in terms of both water level and extent. The model demonstrated the ability to reproduce post-event field measurements. The results and further details of the calibration process are presented in detail in Silvestro et al. (2016).

Direct economic loss computation was done by using the RASOR (Rapid Analysis and Spatialization of Risk) platform (Rudari and the RASOR Team, 2015; Koudogbo et al., 2014) that allows scenario-based impact analysis across different hazards. With respect to floods, the direct economic loss estimation method is based on stage-damage curves, which provide percentage expected loss based on flood depth. Flood damage curves are associated with buildings, according to their flood-relevant features such as occupancy (building usage), height, number of floors above and below the ground and split-level presence. Percentage losses are then multiplied by replacement costs to obtain the economic loss for each building.

This study uses the same damage model configuration described in Silvestro et al. (2016) to compute direct damage to building structure and content. In that study, damage model validation was possible, thanks to the damage data gathered in the aftermath of the 09/10/2014 event: over 3000 citizen claims served as a benchmark for the building-scale damage assessment performed through the RASOR platform. The modelling chain produced the estimate of the total damage with a percentage error of approximately 5%. Damage to vehicles, water and electric systems and transport infrastructure was not considered in the present study.

The RASOR platform was also used recently to quantify monetary flood risk mitigation benefits for the city of Florence (Arrighi et al., 2018).

Potential impacts on population were assessed considering that safety of people can be compromised when exposed to flows that exceed their ability to remain standing and/or traverse a waterway.

Over the last four decades, numerous laboratory-based experimental study regimes (Abt et al., 1989; Karvonen et al., 2000; Jonkman and Penning-Rowsell, 2008; Jonkman et al., 2009; Xia et al., 2014) and

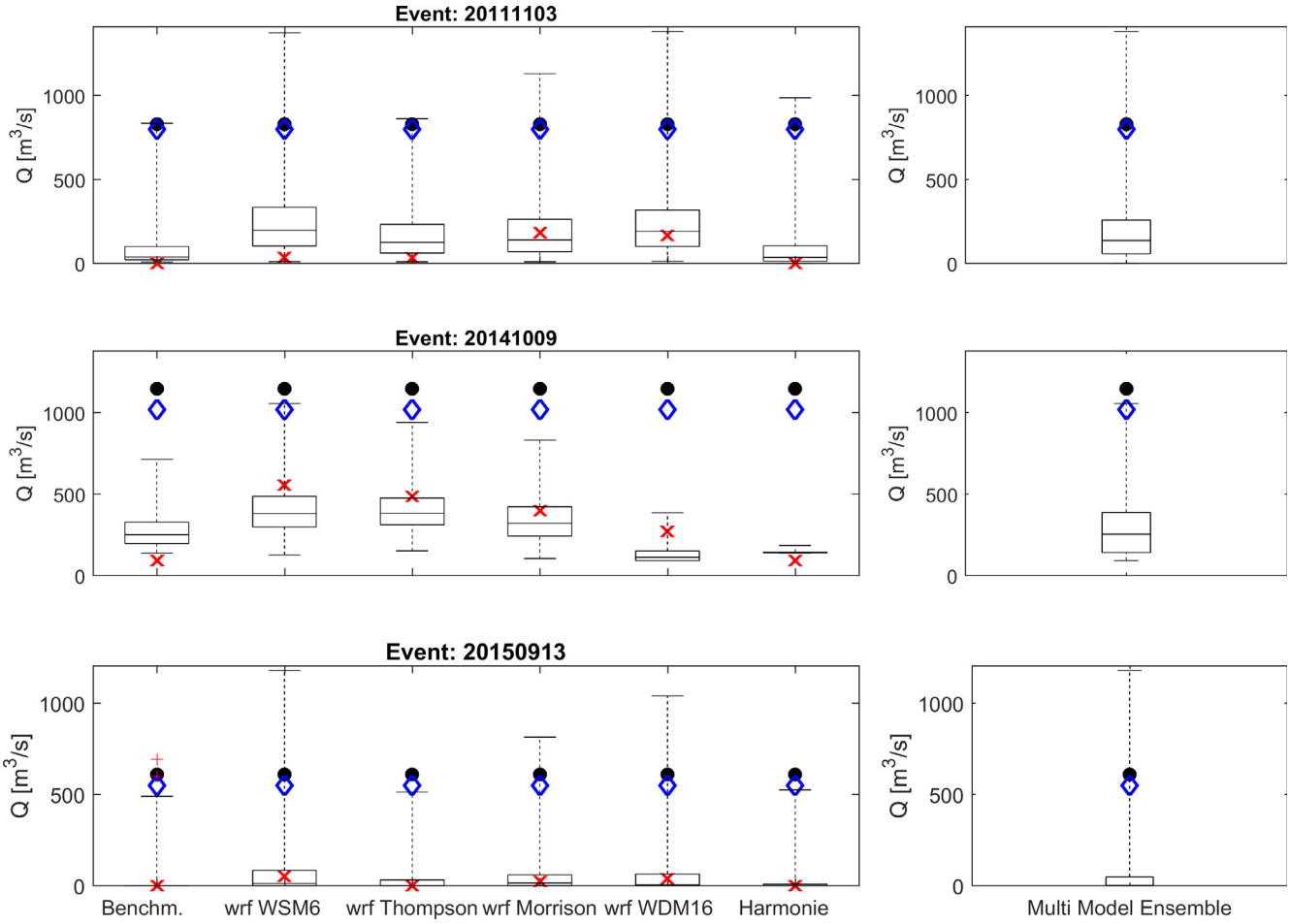

Fig. 5. Results of the flood forecast chain fed with different NWPS for the three considered events. Y-axis reports the peak flow. Panels on the left show the box plot of a single NWPS, while panels on the right report the multi-model ensemble obtained considering all the realizations equi-probable. Blue diamond is the peak flow obtained with the hydrological model fed with observations, black circle is the observed peak flow, red × is the deterministic forecast obtained without downscaling of the precipitation. (For interpretation of the references to colour in this figure legend, the reader is referred to the web version of this article.)

conceptual models (Love, 1987; Lind et al., 2004; Milanesi et al., 2015, Arrighi et al., 2017) have been developed to define the limits of stability within differing flows.

The most common criterion to classify hazard zones is based on different values of the product between the water level H and the water speed U.

In this work, four hazard zones (very high, high, moderate, low flood hazard) were classified considering the thresholds identified by Cox et al. (2010), which consider the instability of adults ("high hazard zone") and children ("moderate hazard zone"). These zones are identified by values of the product $(H{\cdot}U) > 0.8\ m^2s^{-1}$ ("high hazard zone") and $0.4\ m^2s^{-1} < (H{\cdot}U) < 0.8\ m^2s^{-1}$ ("moderate hazard zone"), combined with another condition, independent from the flow velocity, which accounts for the risk of drowning: maximum admissible water depth of 1.2 m for adults and 0.5 m for children. Jonkman et al. (2009), by analysing the loss of life caused by the flooding of New Orleans after Hurricane Katrina, classified a zone with high mortality probability (breach zone) when $(H{\cdot}U) > 5\ m^2s^{-1}$. Based on this threshold an "extreme hazard zone" was added. The resulting four flood hazard zones can be ranked as follows:

- "extreme hazard zone" when $(H{\cdot}U) > 5\ m^2s^{-1}$
- "high hazard zone" when $(H \le 1.2\,m$ and $0.8\ m^2s^{-1} < (H{\cdot}U) \le 5\ m^2s^{-1})$ or $(H > 1.2\,m$ and $(H{\cdot}U) < 5\ m^2s^{-1})$
- "moderate hazard zone" when $(H < 0.5\,m$ and $0.4\ m^2s^{-1} < (H{\cdot}U) \le 0.8\ m^2s^{-1})$ or $(0.5\,m < H < 1.2\,m$ and $(H{\cdot}U) \le 0.8\ m^2s^{-1})$
- "low hazard zone" when $h < 0.5\,m$ and $0\ m^2s^{-1} < (H{\cdot}U) \le 0.4\ m^2s^{-1}$.

2.3. Real-time forecast of damage and population affected

The rigorous method to carry out the damage forecast should be to insert into the flood forecast chain the two ingredients shown in Section 2.2.4: hydraulic modelling and damage estimation. For each streamflow scenario, or at least for all those scenarios that overcome a certain threshold, the hazard map and the damage map should be evaluated using the available models. However, the extended simulation chain that includes damage models would imply an additional amount of computational time and resources, which may delay in time the forecast availability.

The study area is characterized by the fact that the part of the riverbed where the flooding starts is well known: the inlet of the covered channel at approximately 2 km inland from the sea outlet is the most important point where flooding and inundation often begin. This condition is certainly specific, but similar situations are not so unusual in an environment made by small catchments that pass through highly urbanized areas, where such structures as bridges and culverts often cause hydraulic backwater effects.

In this context, we propose an approximate approach that allows substantial saving of computational time, providing reasonable damage estimation in a quick time, also in a probabilistic perspective when

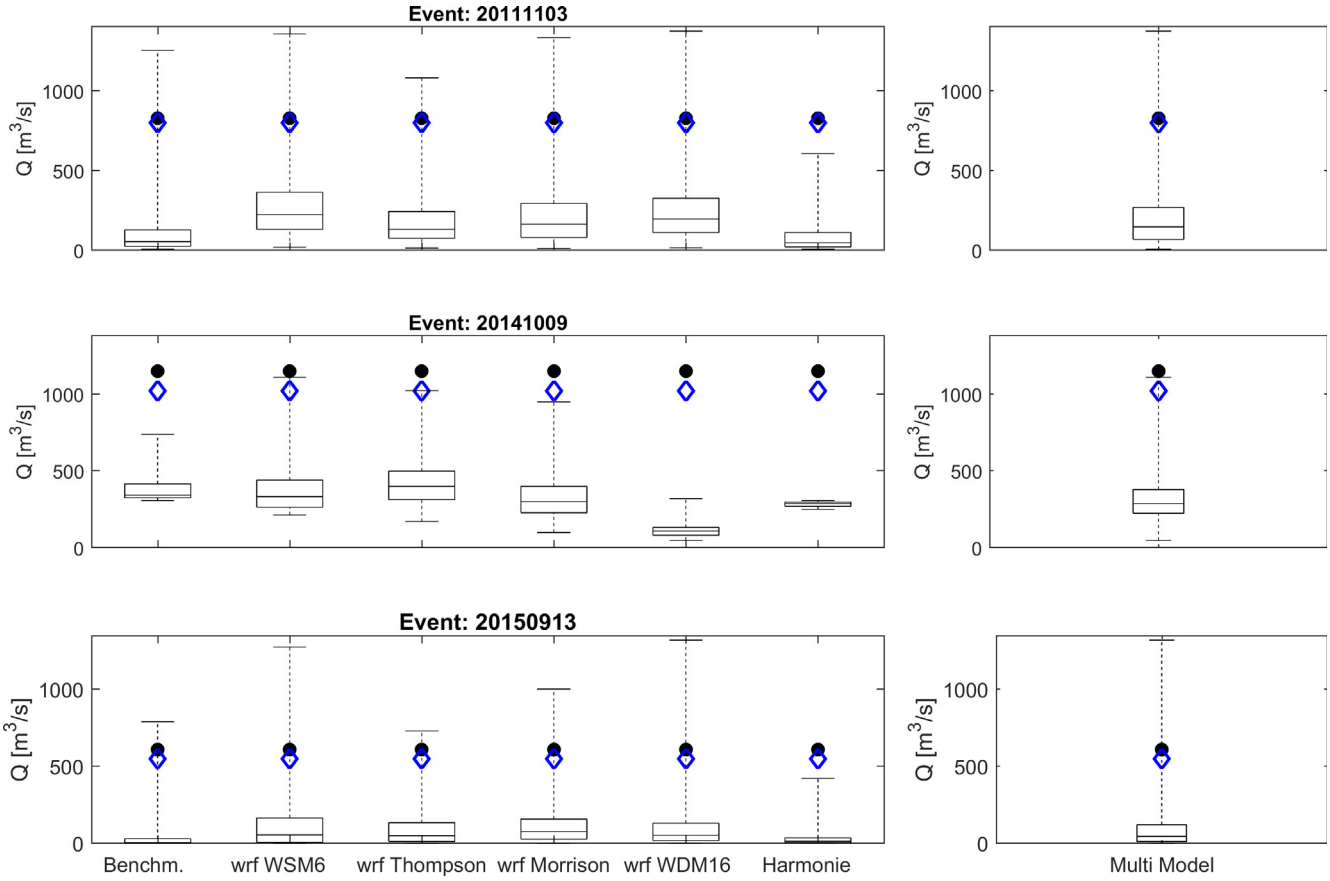

Fig. 6. Results of the flood forecast chain fed with different NWPS and perturbing the initial soil moisture condition for the three considered events. Y-axis reports the peak flow. Panels on the left show the box plot of single NWPS, while panels on the right report the Multi-Model Ensemble obtained considering all realizations equiprobable. Blue diamond is the peak flow obtained with the hydrological model fed with observations, black circle is the observed peak flow. In this case, both uncertainties related to rainfall and soil moisture initial condition are considered. (For interpretation of the references to colour in this figure legend, the reader is referred to the web version of this article.)

multiple streamflow scenarios need to be investigated.

A set of N streamflow scenarios was built using synthetic rainfall events as input to the hydrological model. Hyetographs were built following the approach of Boni et al. (2007): they are studied to have a small increment of a discharge peak between the ith and the ith + 1 scenario around the flooding threshold. Then, the increment increases as the severity of the event increases (Fig. 3).

Each streamflow scenario, with defined peak flow and flooding volume, was used as input for the hydraulic model and the damage model. In this way, a library of damage scenarios was built, and the library relates each peak flow and flooding volume to a damage estimate. This library of preconfigured scenarios is used together with the hydro-meteorological chain to produce probabilistic damage forecast as follows (Fig. 3).

1. Generation of M streamflow scenarios with the probabilistic flood forecast chain.
2. Estimation of peak flow Q_p and flooding volume V_f for each ith scenario that overcomes the flooding threshold.
3. Comparison of Q_p and V_f with those available in the set of N predefined streamflow scenarios. Generally, we will have two comparable scenarios: the first with a similar Q_p and the second V_f.
4. Estimation of two damage scenarios (related to Q_p and V_f) for each ith streamflow scenario that overcomes the flooding threshold. Applying this conservative principle, the larger damage is considered.
5. Build the forecast probabilistic distribution curve of damage.

Relative to the population affected, the previous procedure is applied to identify the scenario, except that the variable to be considered is the affected population instead of economic loss. In other words, step 5 will be replaced by the following:

5bis. Build the forecast probabilistic distribution curve of affected population.

Fig. 3

3. Results

Results are presented referring to the outlet section of Passerella Firpo, where streamflow observations are available. The comparison is carried out referring to the observed peaks, the peaks generated with the hydrological model fed with observations and the peaks obtained by the forecast. The timing of the peak of each ensemble member is not considered. The aggregation scale of NWPS-QPF is 6 h, which is larger than the order of magnitude of the study catchment response time (approximately 2–3 h). The time pattern of each downscaled ensemble member is generated by RainFARM.

Section 3.1.1 focusses on the effects on the streamflow forecast derived by the usage of available high resolution NWPS while in Section 3.1.2, the effects derived by the perturbation of the initial soil moisture condition were introduced. Section 3.2 is instead dedicated to analyse the results of the forecast in terms of impacts: damage and affected population.

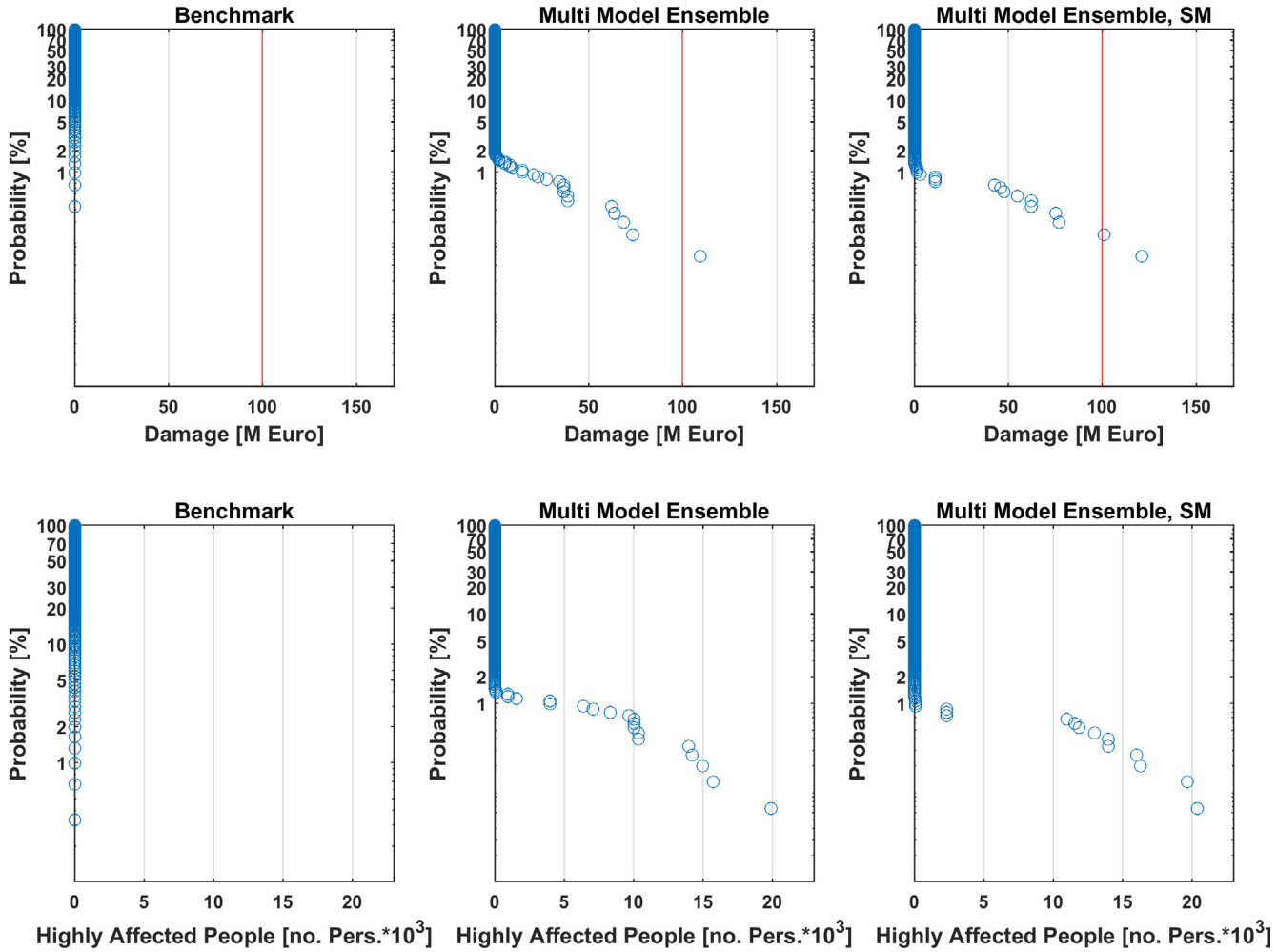

Fig. 7. Event occurred on 09/10/2014. Probability distribution of damage (estimated as sum of damage to structure and damage to content) and affected people. Top panels report the damage distribution of the benchmark compared with those of Multi-Model Ensemble and Multi-Model Ensemble with Soil Moisture uncertainty. Damages are reported in millions of euros. Bottom panels, like the top panels but for "Highly Affected People", the latter is reported in thousands of people. The red line indicates economic damage to buildings modelled with the RASOR platform and validated through citizen claims and municipal authority surveys (Silvestro et al., 2016). (For interpretation of the references to colour in this figure legend, the reader is referred to the web version of this article.)

3.1. Hydrological probabilistic forecast

3.1.1. Assessment of high resolution NWPS

The three considered events (09/10/2014, 04/11/2011 and 14/09/2015) are first re-forecast using the available high resolution NWPS (hereafter HR-NWPS) and comparing the results with those obtained using the operational implementation of the model MOLOCH.

Previous analysis showed that the number of scenarios in the downscaling process of approximately 100 is normally sufficient to investigate the variability of the rainfall field produced by the downscaling (Silvestro and Rebora, 2014). However, 400 downscaled rainfall scenarios are used here. This choice was made to make the results still comparable with what is presented in Section 3.1.2, where two sources of uncertainty were considered: NWPS and soil moisture. In that case, a larger value of M was necessary to describe the variability of the final results adequately in terms of streamflow, when, for instance, superimposing two sources of uncertainties that can lead to contrasting directions (e.g., a very critical rainfall scenario with a dry soil moisture initial condition).

In this case, soil moisture initial conditions are fixed for each event for all the scenarios: they are generated by the run of the hydrological model using the rainfall observations as input.

The probabilistic hydro-meteorological chain accounts for the uncertainties in the rainfall field through the downscaling model.

Fig. 4 helps in understanding how the downscaling algorithm works. Panels a) and b) show the original rainfall field forecast with WRF-WSM6 and an example of the downscaled scenario for the event on 09/10/2014. Panel c) shows the average precipitation accumulated on a box with dimension $2 \cdot S_r$. Rainfall accumulation on t_r is conserved, and the value at times 6, 12, 18, 24 h is the same for all scenarios and equal to the deterministic value (black dotted line). Panel d) shows the average precipitation accumulated on the Bisagno catchment. In this case, the total volume of the NWPS is not conserved, but we have scenarios with larger or lower total accumulation. Panels in Fig. 5 show the results for the three events in terms of box plot representation: on the left column, each panel represents by box plots the probabilistic forecast conditioned to the specific NWP (x-axis) in terms of peak flow (m^3/s). The blue diamond in each box represents the peak flow obtained with the hydrological model fed with observations (hereafter SP) while the black circle is the observed peak flow (hereafter OP). On the right column, panels show the results of all the NWPS together in a Multi-Model Ensemble logic where every single model is given the same weight, so that each peak is considered equi-probable.

Analysing the results for the 09/10/2014 event, the use of HR-NWPS leads in various cases to an improvement in the results with respect to the benchmark considered, confirming the finding of Davolio et al. (2015) and Parodi et al. (2017) that highlighted the benefit provided by increasing the horizontal spatial resolution of NWPS to predict

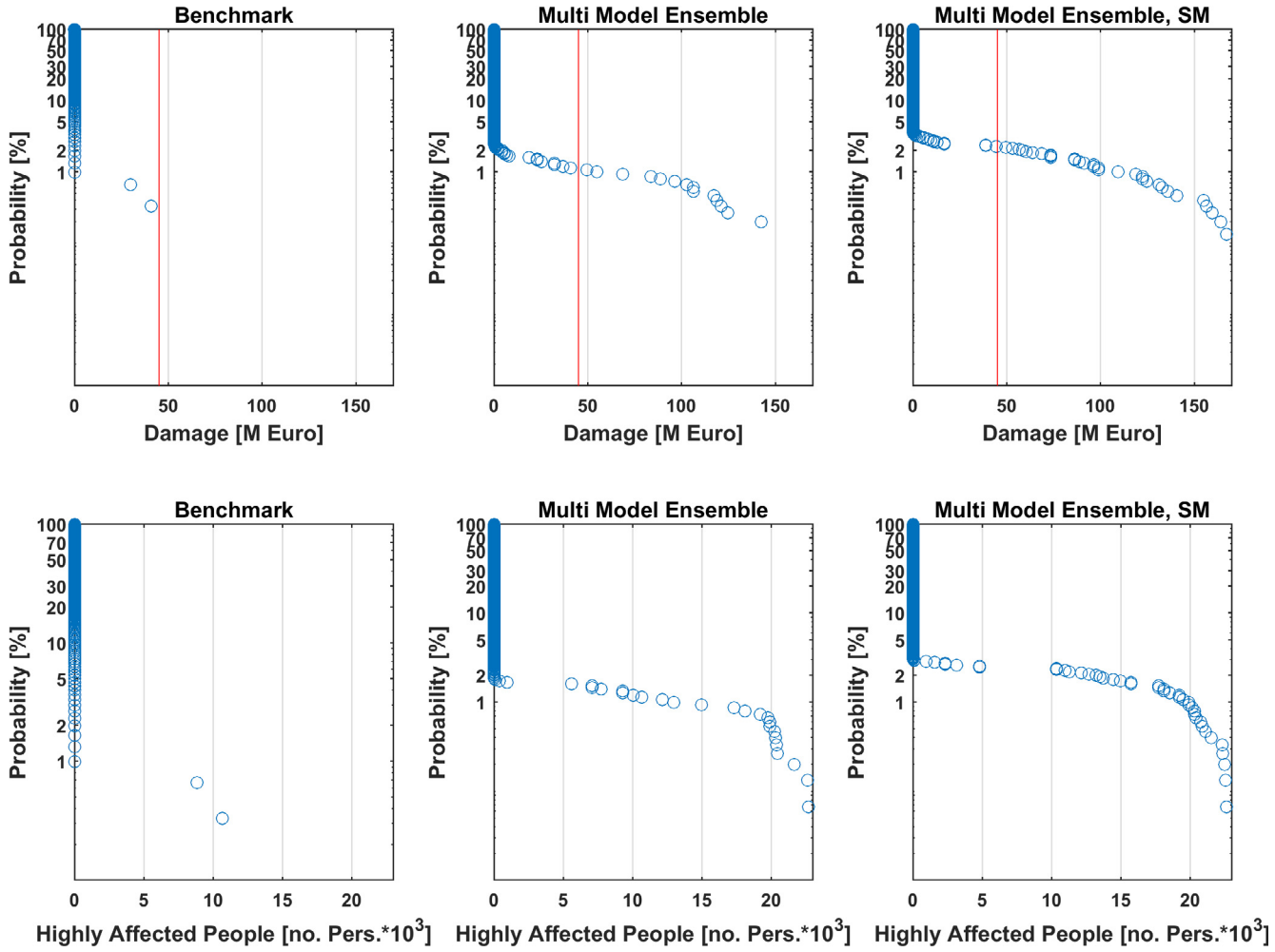

Fig. 8. Same as Fig. 7 for the event that occurred on 04/11/2011.

these kinds of events. Looking at Fig. 5, the range of forecast peak flows increases from a maximum of approximately 700–750 m^3/s provided by the benchmark to values larger than 800 m^3/s and peaking up to 1000 m^3/s for the configuration WRF WSM6 model, which includes also SP. WRF Morrison produces a forecast slightly better than benchmark, only Harmonie and WRF WDM16 did not exhibit an improvement of the forecast. SP and OP are still out of the prediction range in most of the predicted scenarios, but the improvement is evident.

Additionally, for the cases of 04/11/2011 and 14/09/2015, there is an improvement of the forecast for all WRF configurations where WDM16 now appears to be one of the best configurations, while HARMONIE provides predictions similar to the benchmark. The discharge forecast driven by HARMONIE seems not to benefit the SM variability, probably because rainfall patterns and volumes are too different from those that actually occurred.

The deterministic forecast, obtained by feeding the hydrological model directly with rainfall derived by NWPS, is generally poor, confirming the findings of Siccardi et al. (2005). The localization of the forecast precipitation is known to get increasingly important when the basin size decreases. The usage of high-resolution NWPS does not guarantee the correct localization of precipitation, even if the total volume of rainfall is satisfactorily predicted when considered at a larger scale. As a consequence, the flood forecast at basin scale cannot be properly addressed without rainfall downscaling on the study area considered.

In all the study cases, the box plots include the SP and OB only for a reduced number of scenarios, so the expected exceedance probability is generally low. This finding is reasonable and a direct consequence of what was presented by Siccardi et al. (2005) and Silvestro et al. (2011), mainly due to the following causes: i) even when NWPSs make a good prediction of the precipitation volume, in most cases they do not describe the correct spatial and time patterns and/or the rainfall localization; ii) since Bisagno is a small catchment, the reliable aggregation spatial and time scales in the downscaling process (10–20 km and 6 h in this application) are comparable or larger than its size ($\sim 100^{0.5}$ km) and typical response time (~2–3 h). Consequently, only a limited number of scenarios combine rainfall volumes in spatial and the time structures that result in critical parameters for the study catchment. Silvestro et al. (2015a) demonstrated that, even using as input the observed rainfall field, if the aggregation scale increases, then the observed peak is predicted with a decreasing probability. In the present application, we downscale the NWPS rainfall prediction so it is mandatory to use an aggregation spatial scale that is similar to or larger than the Bisagno basin size because of theoretical motivations (Patterson and Orszag, 1971; Siccardi et al., 2005). As a final consideration, we can thus state that the fact of having the observed and simulated peaks in the tail of the predicted peak distribution in most of the presented cases can apparently be considered a poor result, but it must be read accounting for the aforementioned considerations.

Additionally, using a given and predefined HR-NWPS is evidently not sufficient to have a systematic benefit, while the effective strategy for the three considered events seems to use different HR-NWPS or the same HR-NWPS with different physical parameterizations, namely, the use of a multi-model approach. A single model may work well in a

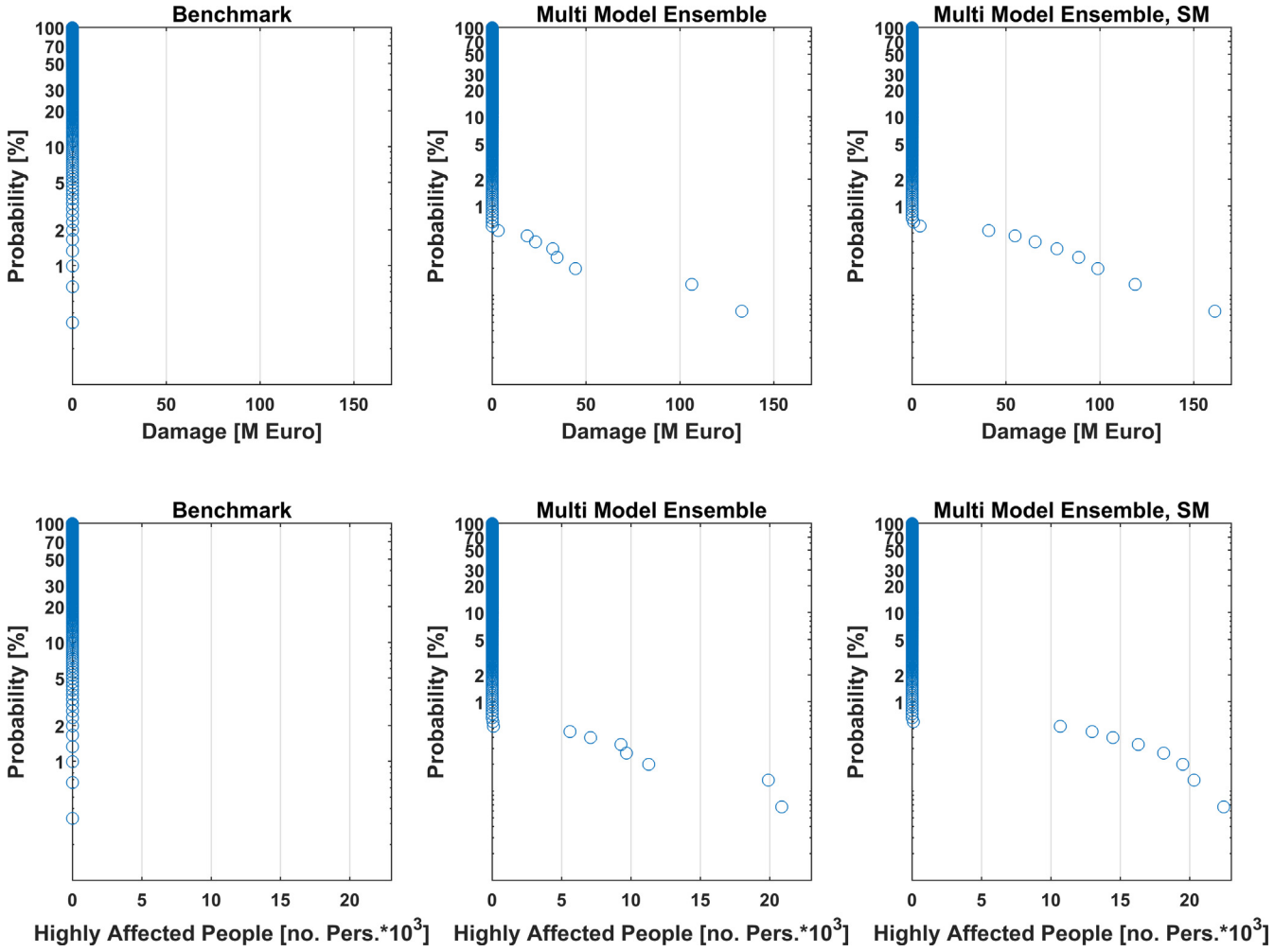

Fig. 9. Same as Fig. 7 for the event that occurred on 14/09/2015.

subset of events but might have bad performance on other case studies (WRF WDM16 works well on 04/11/2011 but not on 09/10/2014). The multi-model approach allows exploring the epistemic uncertainties associated with small scale processes phenomena, which have a great impact on very concentrated and intense rainfall events, causing flash floods.

3.1.2. Assessment of high resolution NWPS and soil moisture uncertainties

As mentioned in the previous section, the differences between SP and OP can be caused by a number of error sources, where initial soil moisture conditions can often drive large errors in streamflow simulations.

In this section, the results of the hydro-meteorological chain accounting for soil moisture initial condition uncertainties (HR-NWPS-SM) are shown. Each downscaled scenario is coupled with an initial soil moisture realization estimated as explained in paragraph 2.2.3. Similar to the previous experiment, the number of rainfall-downscaled scenarios is M = 400.

Analysing the event that occurred on 09/10/2014 (Fig. 6), it is interesting that the Box (25–75 percentile) in some cases is similar to the HR-NWPS case and in some others, HR-NWPS-SM even leads to smaller values of the 75% percentile (wrf WSM6). On the other side, superimposing the two sources of uncertainty allows us to increase the maximum values, thus capturing the SP in the box plot forecast, and in some infrequent cases, peaks are close to OP. The tail of the forecast peak distribution is in fact extended. On the other side, it must be highlighted that the variability of peaks introduced by different NWPSs and by rainfall downscaling is larger than the peak due to soil moisture perturbations.

A similar effect can be noticed also for the other two events (Fig. 6).

3.2. Probabilistic impact forecast: economic losses and people affected

The conversion from streamflow scenarios into damage scenarios and people affected enables the decision maker an in-depth impact analysis of those events that cause some flooding. This transformation involves strong non-linearity, as it depends on urban morphology, which affects flooding dynamics, extension and magnitude. Since the damage is strongly affected by the threshold effect caused by the overbanking level, the results are shown in terms of cumulative distribution that allows a better readability with respect to the box plot representation used in Section 3.1.

Fig. 7 reports distribution of “economic damage” (considering damage to both structure and content) and “highly affected people” distributions for the event on 09/10/2014. The graphs indicate the effects of introducing of the Multi-Model Ensemble approach and those derived from the soil moisture initial condition variability.

The variable “highly affected people” is obtained considering the number of people who reside in high and very high-risk areas, i.e., where flow conditions (water depth and velocity) cause instability to people (see paragraph 2.2.4).

The probability of damage > 0 is approximately 2% (Multi-Model Ensemble) or 1% (Multi-Model Ensemble and Soil Moisture uncertainty). A similar behaviour comes up for the probability of people

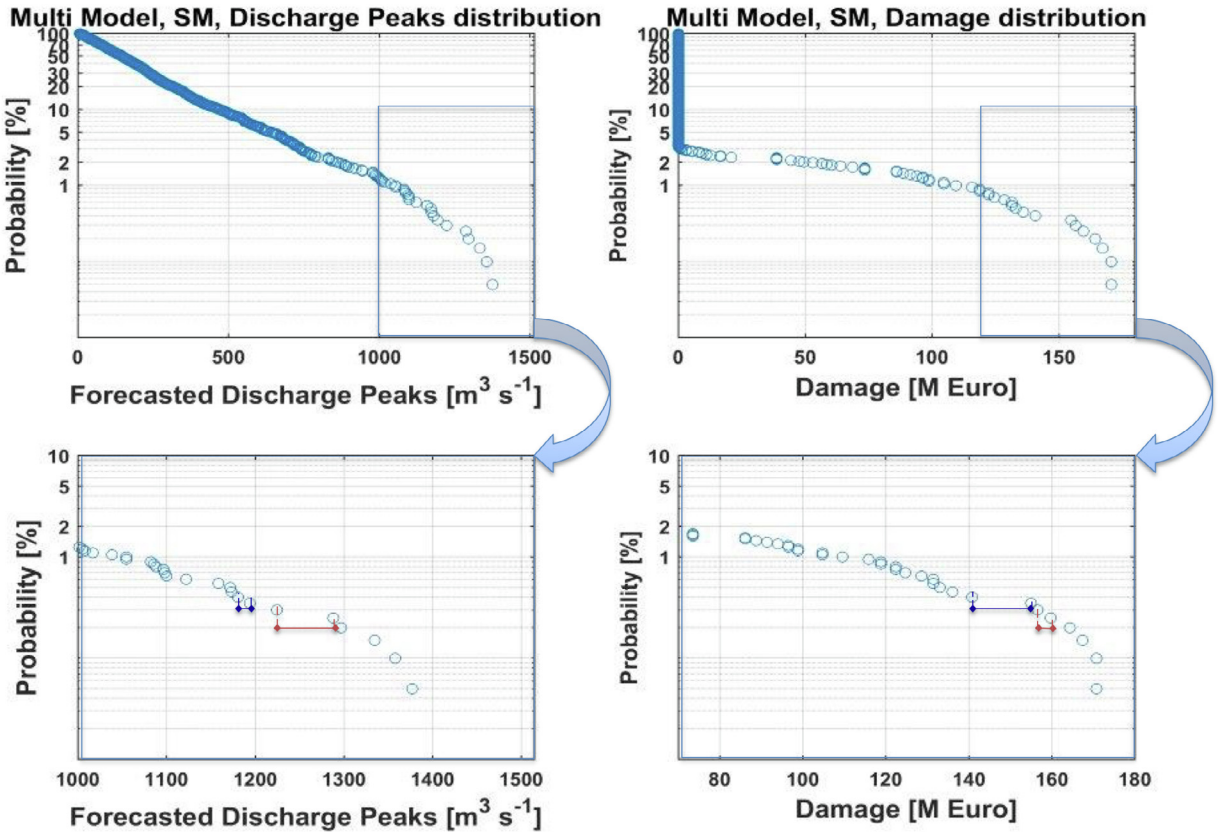

Fig. 10. Distribution of discharge peaks (left panel) and distribution of economic damage to structure and content (right panel). On the second line, a zoom of the distribution tails: small increase in discharge peak can lead to a significant increase in economic losses (blue segments in both panels), while considerable increase in discharge peak may not result in increase of losses (red segment in both panels). (For interpretation of the references to colour in this figure legend, the reader is referred to the web version of this article.)

affected.

Fig. 7 also shows that the Multi-Model includes the estimated real event, which was estimated at approximately 100 Mil. Euro (red point, Silvestro et al., 2016). This occurs even if the observed peak is not included in the forecast. The reason is that the library of scenarios includes at least one streamflow scenario with peak lower than the observed peak but with a similar overtopping volume, thus leading to a similar damage scenario.

In the 04/11/2011 event (Fig. 8), the estimated damage is approximately 45 M euro. This value is estimated without considering the contribution of a small tributary-induced flooding since it is out of the target area of this work but caused a large amount of damage during this event (see Silvestro et al. (2012)). The forecast done using only the operational model (benchmark) defines this scenario as extremely infrequent (probability $< 1\%$) while in the Multi-Model Ensemble damage distribution, it has a probability of approximately 2% and in the Multi-Model Ensemble with Soil Moisture uncertainty, the probability increases between 2% and 5%.

The case of 14/09/2015 has some interesting features (Fig. 9). The streamflow reached a value of approximately 600 m3/s. No inundation occurred, but Bisagno Creek was close to overbanking. The probability of damage and people affected larger than zero was negligible in both the Multi-Model and Model Ensemble with Soil Moisture damage distributions ($< 1\%$). However, it must be admitted that, for the reasons explained in Sections 3.1.1 and 3.1.2, the predicted probabilities of damage > 0 are generally low for all the events. As a consequence, in an operational perspective, it could be not easy to interpret the forecast of 14/09/2015 differently with respect the other two events. The modelling chain considers that the flooding is possible even with very low probability, which could be interpreted as a false alarm.

Analysing the three events in terms of damage, we can conclude that using HR-NWPS seems not sufficient to improve the predictions in the sense that using a unique NWPS with a high resolution does not guarantee that prediction is always and systematically improved.

The results of the forecast chain in terms of impacts confirm, as already shown in Section 3.1, that the multi-model approach seems the most effective strategy to account for meteorological uncertainty instead of using a single model, even if it has a high resolution and a detailed description of the atmospheric processes (i.e., non-hydrostatic, convective permitting). In addition, the results in Figs. 7–9 highlight how the threshold effects introduced by overbanking level affect the damage distribution. Probability of damage is null for all the streamflow scenarios lower than overbanking and then suddenly increases; the probability of damages is always low in the studied events but the magnitude of damage can be huge.

All the considerations presented are valid for the three analysed events that are important case studies (Rebora et al., 2013; Davolio et al., 2017). The test of the complete forecast chain should be continued over a longer period of time, which possibly includes more extreme events, to confirm and generalize the present findings. In other cases, the system may lead to worse results, in particular increasing the false alarms since it accounts for different sources of uncertainties. This kind of verification was not possible because of unavailability of data. Moreover, we believe that a deeper verification would need a specific study, and this is beyond the scope of this study.

4. Conclusions

In this work, a methodology for quantitative real-time impact assessment was presented. The methodology, based on a multi-

meteorological model approach, also considers soil moisture uncertainty and extends the flood forecasting chain to include the quantitative real-time impact assessment in terms of economic losses and affected people. From the analysis of the performances, some interesting and, in our opinion, crucial consideration arose.

Using a multi-model approach that involves different HR-NWPSs improves the hydro-meteorological forecast of the three considered events, confirming the work of Parodi et al. (2017) but also confirming the need for introducing a rainfall downscaling model (Davolio et al., 2015). The benefit of a multi-model approach appears evident, especially considering that there is not a model or a particular model configuration that always performs evidently better than the others. The multi-model approach tries to explore the errors and uncertainties (even if in a partial and coarse way) in meteorological forecasting, while high resolution seems fundamental to capture those very concentrated and intense rainfall events that affect the study area. As discussed in Section 3, the observed event (peak flow) lies always in the tail of the predicted distribution. As a consequence, forecasters and decision makers would have trouble in result interpretation, and they are expected to read results in light of good theoretical preparedness on hydro-meteorological topics.

Accounting for soil moisture initial condition uncertainties helps to improve the results, especially in the 09/10/2014 event, where the methodology increased the probability of success in flood forecasting by increasing the spread of the forecast. To enhance the benefit of superimposing the soil moisture uncertainty in the system, one probably needs to increase the number of the scenario members, increasing the demand on computation.

Results in terms of streamflow prediction appear to be promising, but the availability of data for three events only did not allow a full and extensive validation of the benefit related to the multi-model approach and to the introduction of the soil moisture uncertainty. Specifically, it was not possible to investigate the occurrence of false alarms. Moreover, the adopted scheme for perturbing the soil moisture initial condition is based on a soil status derived by long term simulation. For the sake of clarity, the method does not allow consideration of space and time errors of the hydrological model. Thus, as a consequence, it could fail to properly account for the uncertainty in some situations.

Second, the proposed methodology underlines the importance of the availability of an impact forecast. The transition from streamflow forecast to impact forecast in terms of economic damages and affected people increases the amount of available information for the decision-making process. Considering only the discharge peak distribution (Fig. 10, left panel), the decision maker cannot obtain precise information on the flood impact after overtopping. When comparing the distribution of discharge peaks (Fig. 10, left panel) to the related distribution of economic damage to structure and content (Fig. 10, right panel), a strong non-linearity in this conversion is found, as expected. A small increase in discharge peak can lead to a significant increase in losses, as highlighted by the blue segment, and vice versa, considerable increase in discharge peak may result in a minor increase in losses (red segment). The reason for this behaviour can be explained easily, considering that the dynamics of the inundation strongly depend on urban morphology, and the discharge peak is not the only influencing parameter, but the shape of the hydrograph and the inundation volume also play an important role.

Economic loss distribution can be compared with reference thresholds such as the cost of warning civil protection staff and population, availability of emergency funds or a portion of city GDP considered critical for city economy. The decision maker can read from the graph the probability to exceed one of these economic thresholds.

A crucial point of the work presented is related to the estimation of impacts and damages caused by the flash floods, since the flash floods are essential to calibrate and validate the models. In this application, we used field measurements as well citizen claims of the damages suffered. The post flash-flood surveys have a key role as evidenced in some studies that emphasized the usefulness of data and information derived from post-event analysis (Marchi et al., 2009; Marchi et al., 2010).

A possible future extension and application of this methodology may consider a regional approach. Given 1) the size of the watershed of the Ligurian coast, 2) the uncertainty in predicting the location of the meteorological event, and 3) warning messages are issued for a homogeneous “warning area” and not for a single site, it would be possible to compute impact losses for all watersheds belonging to the same warning area. Then, a decision criterion may compare the probability of having losses with the cost of activation for the whole warning area. This probability can be substantially higher with respect to the one computed in a single site, while the cost of warning messages and activation for the warning area may increase more smoothly (some costs of single site activation are the same for the warning area activation).

In any case, a decision-making process that includes impact forecast (economic loss, affected population) instead of hazard parameters (discharge) alone would require a substantial modification of current Early Warning Systems setup and related standard operating procedures, which may delay its adoption by decision makers.

Acknowledgements

This work is supported by IMPREX Horizon 2020 project, the Italian Civil Protection Department and by the Italian Region of Liguria. We are very grateful to all the meteorologists and the hydrologists of the Meteo-Hydrologic Centre of the Liguria Region (in particular, Matteo Corazza and Francesca Giannoni), for the many useful discussions we had and for the time spent to furnish us data. We are finally very grateful to SMHI personnel, in particular, Magnus Lindskog and Ilias Pechlivanidis, for the collaboration among IMPREX project especially for sharing HARMONIE NWPS re-forecasts.

References

Abt, S.R., Wittler, R.J., Taylor, A., Love, D.J., 1989. Human Stabil- ity in a High Flood Hazard Zone1. J. Am. Water Resour. As. 25, 881–890. https://doi.org/10.1111/j.1752-1688.1989.tb05404.x.

Arrighi, C., Oumeraci, H., Castelli, F., 2017. Hydrodynamics of pedestrians' instability in floodwaters. Hydrol. Earth Syst. Sci. 21. https://doi.org/10.5194/hess-21-515-2017.

Arrighi, Chiara, Rossi, Lauro, Trasforini, Eva, Rudari, Roberto, Ferraris, Luca, Brugioni, Marcello, Franceschini, Serena, Castelli, Fabio, 2018. Quantification of flood risk mitigation benefits: A building-scale damage assessment through the RASOR platform. J. Environ. Manage. 207, 92–104. https://doi.org/10.1016/j.jenvman.2017.11.017.

Bauer, S., 1974. A modified Horton equation during intermittent rainfall. Hydrol. Sci. Bull. 19, 219–229.

Bengtsson, L., Andrae, U., Aspelien, T., Batrak, Y., Calvo, J., de Rooy, W., Gleeson, E., Hansen-Sass, B., Homleid, M., Hortal, M., Ivarsson, K.-I., Lenderink, G., Niemelä, S., Pagh-Nielsen, K., Onvlee, J., Rontu, L., Samuelsson, P., Santos-Muñoz, D., Subias, A., Tijm, S., Toll, V., Yang, X., Ödegaard-Költzow, M., 2017. The HARMONIE-AROME model configuration in the ALADIN-HIRLAM system. Mon. Wea. Rev 10.1175/MWR-D-16-0417.1.

Boni, G., Ferraris, L., Giannoni, F., Roth, G., Rudari, R., 2007. Flood probability analysis for un-gauged watersheds by means of a simple distributed hydrologic model. Adv. Water Resour. 30 (10), 2135–2144. https://doi.org/10.1016/j.advwatres.2006.08.009.

Brussolo, E., von Hardenberg, J., Ferraris, L., Rebora, N., Provenzale, A., 2008. Verification of quantitative precipitation forecasts via stochastic downscaling. J. Hydrometeor. 9, 1084–1094.

Cenci, L., Laiolo, P., Gabellani, S., Campo, L., Silvestro, F., Delogu, F., Boni, G., Rudari, R., 2016. Assimilation of H-SAF soil moisture products for flash flood early warning systems. Case study: mediterranean catchments. IEEE J. Sel. Top. Appl. Earth.

Cole, Steven J., Moore, Robert J., Wells, Steven C., Mattingley, Paul S., Lang, M., Klijn, F., Samuels, P., 2016. Real- time forecasts of flood hazard and impact: some UK experiences. E3S Web Conf. 7, 18015. https://doi.org/10.1051/e3sconf/20160718015.

Cox, R.J., Shand, T.D., Blacka, M. J. Australian Rainfall & Runoff, Revision Project 10: Appropriate Safety Criteria for Peo- ple, Stage 1 Report, 2010.

Davolio, S., Silvestro, F., Malguzzi, P., 2015. Effects of increasing horizontal resolution in a convection permitting model on flood forecasting: The 2011 dramatic events in Liguria (Italy). J. Hydrometeor. 16, 1843–1856. https://doi.org/10.1175/JHM-D-14-0094.1.

Davolio, S., Silvestro, F., Gastaldo, T., 2017. Impact of rainfall assimilation on high-resolution hydro-meteorological forecasts over Liguria (Italy). J. Hydrometeor. 18,

2659–2680. https://doi.org/10.1175/JHM-D-17-0073.1.
Dickinson, R., 1988. The force-restore method for surface temperature and its generalization. J. Clim. 1, 1086–1097.
Diskin, M.H., Nazimov, N., 1994. Linear reservoir with feedback regulated inlet as a model for the infiltration process. J. Hydrol. 172, 313–330.
Dottori, F., Kalas, M., Salamon, P., Bianchi, A., Alfieri, L., 2017. An operational procedure for rapid flood risk assessment in Europe. Nat. Hazards Earth Syst. Sci. 17 (7), 1111–1126.
European Environment Agency (EEA), "Floodplain management: reducing flood risks and restoring healthy ecosystems", available at https://www.eea.europa.eu/highlights/floodplain-management-reducing-flood-risks, 2016.
Fiori, E., Comellas, A., Molini, L., Rebora, N., Siccardi, F., Gochis, D.J., Tanelli, S., Parodi, A., 2014. Analysis and hindcast simulations of an extreme rainfall event in the Mediterranean area: the Genoa 2011 case. Atmos. Res. 138, 13–29.
Fiori, E., Ferraris, L., Molini, L., Siccardi, F., Kranzlmueller, D., Parodi, A., 2017. Triggering and evolution of a deep convective system in the Mediterranean Sea: Modelling and observations at a very fine scale. Q. J. R. Meteorol. Soc. 143, 927–941. https://doi.org/10.1002/qj.2977.
Gabellani, S., Silvestro, F., Rudari, R., Boni, G., 2008. General calibration methodology for a combined Horton-SCS infiltration scheme in flash flood modeling. Nat. Hazards Earth Science 8, 1317–1327.
Gourley, J.J., Flamig, Z.L., Hong, Y., Howard, K.W., 2014. Evaluation of past, present and future tools for radar-based flashflood prediction in the USA. Hydrolog. Sci. J. 59, 1377–1389. https://doi.org/10.1080/02626667.2014.919391.
Gourley, J., Flamig, Z., Vergara, H., Kirstetter, P.-E., Clark, R., Argyle, E., Arthur, A., Martinaitis, S., Terti, G., Erlingis, J., Hong, Y., Howard, K., 2017. The Flash project: improving the tools for flash flood monitoring and prediction across the United States. B. Am. Meteorol. Soc. 98, 361–372.
Giannoni, F., Roth, G., Rudari, R., 2000. A Semi – Distributed Rainfall – Runoff Model Based on a Geomorphologic Approach. Physics and Chemistry of the Earth.
Giannoni, F., Roth, G., Rudari, R., 2005. A procedure for drainage network identification from geomorphology and its application to the prediction of the hydrologic response. Adv. Water Resour. 28 (6), 567–581. https://doi.org/10.1016/j.advwatres.2004.11.013.
Hally, A., Caumont, O., Garrote, L., Richard, E., Weerts, A., Delogu, F., Fiori, E., Rebora, N., Parodi, A., Mihalovic, A., Ivkovic, M., Dekic, L., van Verseveld, W., Nuissier, O., Ducrocq, V., D'Agostino, D., Galizia, A., Danovaro, E., Clematis, A., 2015. Hydrometeorological multi-model ensemble simulations of the 4 November 2011 flash-flood event in Genoa, Italy, in the framework of the DRIHM project. Nat. Hazards Earth Syst. Sci. 15 (3), 537–555.
Hong, S.-Y., Lim, J.-O.J., 2006. The WRF single-moment 6-class microphysics scheme (WSM6). J. Korean Meteor. Soc. 42, 129–151.
Jonkman, S.N., Penning-Rowsell, E., 2008. Human instability in flood flows. J. Am. Water Resour. As. 44, 1208–1218. https://doi.org/10.1111/j.1752-1688.2008.00217.x.
Jonkman, S.N., Maaskant, B., Boyd, E., Levitan, M.L., 2009. Loss of life caused by the flooding of new Orleans after hurricane Katrina: analysis of the relationship between flood characteristics and mortality. Risk Anal. 29, 676–698. https://doi.org/10.1111/j.1539-6924.2008.01190.x.
Karvonen, R. A., Hepojoki, H. K., Huhta, H. K., and Louhio, A.: The use of physical models in dam-break analysis, RESCDAM Final Report, Helsinki University of Technology, Helsinki, Finland, available at: https://www.google.it/url?sa (last access: 24 January 2017), 2000.
Koudogbo, F.N., Duro, J., Rossi, L., Rudari, R., Eddy, A., 2009. Multi-hazard risk analysis using the FP7 RASOR Platform. Proc. SPIE XVI, 92390J. https://doi.org/10.1117/12.2067444, 2014.
Laiolo, P., Gabellani, S., Rebora, N., Rudari, R., Ferraris, L., Ratto, S., Stevenin, H., Cauduro, M., 2014. Validation of the Flood-PROOFS probabilistic forecasting system. Hydrol. Process. 28, 3466–3481. https://doi.org/10.1002/hyp.9888.
Laiolo, P., Gabellani, S., Campo, L., Silvestro, F., Delogu, F., Rudari, R., Pulvirenti, L., Boni, G., Fascetti, F., Pierdicca, N., Crapolicchio, R., Hasenauer, S., Puca, S., 2016. Impact of different satellite soil moisture products on the predictions of a continuous distributed hydrological model. Int. J. Appl. Earth Obs. Geoinf. 48, 131–145. https://doi.org/10.1016/j.jag.2015.06.002.
Lagasio, M., Parodi, A., Procopio, R., Rachidi, F., Fiori, E., 2017. Lightning Potential Index performances in multimicrophysical cloud-resolving simulations of a back-building mesoscale convective system: The Genoa 2014 event. J. Geophys. Res.: Atmospheres 122 (8), 4238–4257.
Le Bihan, G., Payrastre, O., Gaume, E., Moncoulon, D., Pons, F., 2016. Regional models for distributed flash-flood nowcasting: towards an estimation of potential impacts and damages. E3S Web Conf., 7, 18013. https://doi.org/10.1051/e3sconf/20160718013.
Le Bihan, G., Payrastre, O., Gaume, E., Moncoulon, D., Pons, F., 2017. The challenge of forecasting impacts of flash floods: test of a simplified hydraulic approach and validation based on insurance claim data. Hydrol. Earth Syst. Sci. 21, 5911–5928. https://doi.org/10.5194/hess-21-5911-2017.
Lim, K.-S.S., Hong, S.-Y., 2010. Development of an effective double-moment cloud microphysics scheme with prognostic cloud condensation nuclei (CNN) for weather and climate models. Mon. Wea. Rev. 138, 1587–1612.
Lind, N., Hartford, D., Assaf, H., 2004. Hydrodynamic models of Hu- man Stability in a Flood. J. Am. Water Resour. As. 8, 89–96.
Love, D.J., 1987. Analysis of a high hazard flood zone. Technical Report prepared for City of Boulder Public Works Department, Boulder, Colorado.
Marchi, L., Borga, M., Preciso, E., Sangati, M., Gaume, E., Bain, V., Delrieu, G., Bonnifait, L., Pogancik, N., 2009. Comprehensive post-event survey of a flash flood in Western Slovenia: observation strategy and lessons learned. Hydrol. Process. 23 (26), 3761–3770. https://doi.org/10.1002/hyp.7542.
Marchi, L., Borga, M., Preciso, E., Gaume, E., 2010. Characterisation of selected extreme flash floods in Europe and implications for flood risk management. J. Hydrol. https://doi.org/10.1016/j.jhydrol.2010.07.017.
Mascaro, G., Vivoni, E.R., Deidda, R., 2010. Implications of ensemble quantitative precipitation forecast errors on distributed streamflow forecasting. J. Hydrometeorol. 11, 69–86. https://doi.org/10.1175/2009JHM1144.1.
Milanesi, L., Pilotti, M., Ranzi, R., 2015. A conceptual model of people's vulnerability to floods. Water Resour. Res. 7206–7230. https://doi.org/10.1002/2014 WR016172.
Molinari, D., Handmer, J., 2011. A behavioural model for quantifying flood warning effectiveness. J. Flood Risk Manage. 4, 23–32.
Molini, L., Parodi, A., Siccardi, F., 2009. Dealing with uncertainty: an analysis of the severe weather events over Italy in 2006. Nat. Hazards Earth Syst. Sci. 9, 1–13.
Morrison, H., Pinto, J.O., 2005. Mesoscale modeling of springtime Arctic mixed-phase stratiform clouds using a new two-moment bulk microphysics scheme. J. Atmos. Sci. 62, 3683–3704.
Morrison, H., Pinto, J.O., 2006. Intercomparison of bulk microphysics scheme in mesoscale simulations of springtime Arctic mixedphase stratiform clouds. Mon. Wea. Rev. 134, 1880–1900.
Naulin, J.-P., Payrastre, O., Gaume, E., 2013. Spatially distributed flood forecasting in flash flood prone areas: Application to road network supervision in Southern France. J. Hydrol. 486, 88–99. https://doi.org/10.1016/j.jhydrol.2013.01.044.
Nielsen, K.P., Gleeson, E., Rontu, L., 2014. Radiation sensitivity tests of the HARMONIE 37 h1 NWP model. Geosci. Model Dev. 7, 1433–1449. https://doi.org/10.5194/gmd-7-1433-2014.
Parodi, A., Kranzlmueller, D., Clematis, A., Danovaro, E., Galizia, A., Garrote, L., Llasat, M.C., Caumont, O., Richard, E., Harpham, Q., Siccardi, F., Ferraris, L., Rebora, N., Delogu, F., Fiori, E., Molini, L., Foufoula-Georgiou, E., D'Agostino, D., 2017. DRIHM (2US): an e-Science environment for hydro-meteorological research on high impact weather events. Bull. Amer. Meteor. Soc. https://doi.org/10.1175/BAMS-D-16-0279.1. in press.
Patterson, G., Orszag, S., 1971. Spectral calculations of isotropic turbulence: efficient removal of aliasing interaction. Phys. Fluids 14, 2538–2541.
Rebora, N.L., Ferraris, J.H., 2006a. Hardenberg and Provenzale, A.: Rainfall downscaling and flood forecasting: a case study in the Mediterranean area. Nat. Hazards and Earth Syst. Sci. 6, 611–619.
Rebora, N., Ferraris, L., Hardenberg, J.H., Provenzale, A., 2006. The RainFARM: Rainfall Downscaling by a Filtered Auto Regressive Model. J. Hydrometeorol. 7 (4), 724–738.
Rebora, N., Molini, L., Casella, E., Comellas, A., Fiori, E., Pignone, F., Siccardi, F., Silvestro, F., Tanelli, S., Parodi, A., 2013. Extreme rainfall in the mediterranean: What can we learn from observations? J. Hydrometeorol. 14, 906–922.
Rudari, R., 2015. The RASOR Team: RASOR Project: Rapid Analysis and Spatialisation of Risk, from Hazard to Risk using EO data. Geophys. Res. Abstr. 17 EGU2015-2538, EGU General Assembly 2015.
Sai, F., Lydia, Cumiskey L., Weerts, A., Biswa, Bhattacharya B., Raihanul, Haque Khan, 2018. Towards impact-based flood forecasting and warning in Bangladesh: a case study at the local level in Sirajganj district. Nat. Hazards Earth Syst. Sci. Discuss https://doi.org/10.5194/nhess-2018-26, Manuscript under review for journal Nat. Hazards Earth Syst. Sci. (discussion started: 19 February 2018).
Sättele, M., Bründl, M., Straub, D., 2016. Quantifying the effectiveness of early warning systems for natural hazards. Nat. Hazards Earth Syst. Sci. 16, 149–166. https://doi.org/10.5194/nhess-16-149-2016.
Schroeder, A., Gourley, J., Henderson, J., Parhi, P., Rahmani, V., Reed, K., Schumacher, R., Smith, B.K., Taraldsen, M., 2016. The development of a flash flood severity index. J. Hydrol. 541, 523–532. https://doi.org/10.1016/j.jhydrol.2016.04.005.
Siccardi, F., Boni, G., Ferraris, L., Rudari, R., 2005. A hydro-meteorological approach for probabilistic flood forecast. J. Geophys. Res 110, d05101. https://doi.org/10.1029/2004jd005314.
Silvestro, F., Rebora, N., Ferraris, L., 2011. Quantitative flood forecasting on small and medium size basins: a probabilistic approach for operational purposes. J. Hydrometeorol. 12 (6), 1432–1446.
Silvestro, F., Gabellani, S., Giannoni, F., Parodi, A., Rebora, N., Rudari, R., Siccardi, F., 2012. A Hydrological Analysis of the 4th November 2011 event in Genoa. Nat. Hazards earth syst. Sci. 12, 2743–2752. https://doi.org/10.5194/nhess-12-2743-2012.
Silvestro, F., Gabellani, S., Delogu, F., Rudari, R., Boni, G., 2013. Exploiting remote sensing land surface temperature in distributed hydrological modelling: the example of the Continuum model. Hydrol. Earth Syst. Sci. 17, 39–62. https://doi.org/10.5194/hess-17-39-2013.
Silvestro, F., Rebora, N., 2014. Impact of precipitation forecast uncertainties and initial soil moisture conditions on a probabilistic flood forecasting chain. J. Hydrol. 519, 1052–1067.
Silvestro, F., Rebora, N., Giannoni, F., Cavallo, A., Ferraris, L., 2015a. The flash flood of the Bisagno Creek on 9th October 2014: an "unfortunate" combination of spatial and temporal scales. J. Hydrol. https://doi.org/10.1016/j.jhydrol.2015.08.004.
Silvestro, F., Gabellani, S., Delogu, F., Rudari, R., Laiolo, P., Boni, G., 2015b. Uncertainty reduction and parameter estimation of a distributed hydrological model with ground and remote-sensing data. Hydrol. Earth Syst. Sci. 19, 1727–1751. https://doi.org/10.5194/hess-19-1727-2015.
Silvestro, F., Rebora, N., Rossi, L., Dolia, D., Gabellani, S., Pignone, F., Trasforini, E., Rudari, R., De Angeli, S., Masciulli, C., 2016. What if the 25 October 2011 event that struck Cinque Terre (Liguria) had happened in Genoa, Italy? Flooding scenarios, hazard mapping and damage estimation. Nat. Hazards Earth Syst. Sci. 16, 1737–1753. https://doi.org/10.5194/nhess-16-1737-2016.
Simmons, A.J., Burridge, D.M., Jarraud, M., Girard, C., Wergen, W., 1989. The ECMWF medium-range prediction models development of the numerical formulations and the impact of increased resolution. Meteorol. Atmos. Phys. 40 (1–3), 28–60.

Thompson, G., Field, P.R., Rasmussen, R.M., Hall, W.D., 2008. Explicit forecast of winter precipitation using an improved bulk microphysics scheme. Part II: Implementation of a new snow parameterization. Mon. Weather Rev. 136, 5095–5115. https://doi.org/10.1175/2008MWR2387.1.

Todini, E., Ciarapica, L., 2001. The TOPKAPI Model. Mathematical Models of Large Watershed Hydrology. In: Singh, V.P. (Ed.), Water Resources Publications, Littleton, Colorado, Chapter 12.

Versini, P.-A., Berenguer, M., Corral, C., Sempere-Torres, D., 2014. An operational flood warning system for poorly gauged basins: demonstration in the Guadalhorce basin (Spain). Nat. Hazards 71, 1355–1378. https://doi.org/10.1007/s11069-013-0949-7.

World Meteorological Organization (WMO): Guidelines on Multi-hazard Impact-based Forecast and Warning Services, ISBN 978-92-63-11150-0, 2015.

Wooding, R.A., 1965. A hydraulic modeling of the catchment-stream problem. 1. Kinematic wave theory. J. Hydrol. 3, 254–267.

Xia, J., Falconer, R.A., Wang, Y., Xiao, X., 2014. New criterion for the stability of a human body in floodwaters. J. Hydraul. Res. 52, 93–104. https://doi.org/10.1080/00221686.2013.875073.

Zappa, M., Jaun, S., Germann, U., Walser, A., Fundel, F., 2011. Superposition of three sources of uncertainties in operational flood forecasting chains. Atmos. Res. https://doi.org/10.1016/j.atmosres.2010.12.005.